INSTITUTE OF PHYSICS PUBLISHING PLASMA PHYSICS AND CONTROLLED FUSION

Plasma Phys. Control. Fusion **48** (2006) S137–S153 doi:10.1088/0741-3335/48/4/S10

Observation of zonal flow-like structures using the autocorrelation-width technique

A Bencze[1], M Berta[2], S Zoletnik[1], J Stockel[3], J Adámek[3] and M Hron[3]

[1] KFKI-RMKI, Association EURATOM, PO Box 49, H-1525 Budapest, Hungary
[2] Széchenyi István University, Association EURATOM, Győr, Hungary
[3] IPP, Association EURATOM, Prague, Czech Republic

Received 2 September 2005, in final form 25 January 2006
Published 21 March 2006
Online at stacks.iop.org/PPCF/48/S137

Abstract

This paper presents the first application of the autocorrelation-width technique (Bencze A and Zoletnik S 2005 *Phys. Plasmas* **12** 052323) to detect and characterize the microturbulence-zonal flow system using fluctuating signals ($\tilde{\phi}_f$, $\tilde{I}_s$) measured by arrays of single-tip Langmuir probes in the CASTOR tokamak. Radially localized (≈1 cm) random flow structures have been clearly observed with a lifetime of ≈1 ms and a long-range poloidal correlation, extending over at least one-fourth of the poloidal circumference.

(Some figures in this article are in colour only in the electronic version)

1. Introduction

At present it is generally accepted by the fusion community that the understanding of the drift wave–zonal flow turbulence plays a crucial role in the understanding and handling of anomalous transport and different spontaneous transitions of the collective plasma state in the plasma core.

Theoretically the drift wave (DW) turbulence consists of unstable potential modes ($\boldsymbol{k}$, ω), with $k_\parallel \ll k_\perp \gg 1/L_\perp$ and $\omega \ll \Omega_{ci}$, where ($\parallel$, $\perp$) denote directions with respect to the confining magnetic field, $L_\perp$ is the perpendicular macroscopic size of the system and $\Omega_{ci} = eB/m_i$ is the ion cyclotron frequency. The free energy sources of DW instability are the gradients of macroscopic profiles (density, temperature, etc). The 'equilibrium' spectrum of the fully developed DW turbulence can be unstable in the presence of random shear flows or zonal flows (ZF) which are electrostatic potential modes with $(k_r, k_\theta, k_\phi) = (k_r, 0, 0)$. The effect of shearing on the drift waves can be described as a diffusion of the DW radial wave number in $\boldsymbol{k}$-space. In order to conserve drift wave action density, the increase in the DW radial wave number causes a decrease in DW energy and as the energy of the zonal flow–drift wave system must be conserved a zonal flow growth will arise. It has to be noted that the excitation of ZF modes—mediated by the radial gradient of the DW turbulent Reynolds stress—is a completely nonlinear, but generic process in 2D turbulence called the 'inverse cascade'. For comprehensive reviews on the topic of DW–ZF turbulence we refer the reader to [1, 2].

The appearance of ZFs and its effect on regulating turbulent transport was first observed in numerical simulations at fluid, gyro-fluid and gyro-kinetic levels [3–7].

First experimental investigations, which were devoted to the detection of sheared zonal flows and clarification of their connection to turbulence level and transport, followed the theory with a delay of almost a decade. It was shown by Hidalgo *et al* [8] that the electrostatic component of the Reynolds stress (R_s) has a significant gradient ($\mathrm{d}R_s/\mathrm{d}r \approx 10^7$–$10^8\,\mathrm{m\,s^{-2}}$) close to the velocity shear layer location. Following this line at the HT-6M tokamak Xu and co-workers [9] measuring the time evolution of the turbulence-induced Reynolds stress gradient across the L–H transition found a strong correlation between the enhanced $\partial_r R_s$ and the poloidal flow acceleration. Recently the main terms entering the momentum balance have been measured in an RFP configuration [10]. The complete Reynolds stress was found to be the main term opposing the action of the viscosity and then driving the shear of $\boldsymbol{E} \times \boldsymbol{B}$ velocity. The problem of flow generation can be reformulated as a three-wave mode-coupling problem [11, 12], transforming the search for Reynolds stress profile changes into the study of the bispectrum of the potential fluctuations. Such nonlinear signal processing was done by Moyer *et al* [13] using turbulence data acquired in neutral beam heated discharges with spontaneous L–H transitions in the DIII-D tokamak. The results showed a transient increase in the three-wave coupling between low and high frequencies just before and during the L–H transition.

The first indirect experimental identification of zonal flows using phase-contrast imaging of density fluctuations in the DIII-D tokamak was done by Coda *et al* [14]. The BES measurements and the time-delay-estimation analysis of Jakubowski *et al* [15] pointed to the existence of low frequency ($\approx$15 kHz), nearly coherent oscillations in the poloidal flow. Such flows have been observed earlier in the 3D Braginskii simulations [16] as a coherent branch of ($m = 0, n = 0$) zonal flows called geodesic acoustic modes (GAM). The existence of GAM modes was also reported by Conway *et al* [17] at ASDEX by means of Doppler reflectometry. Last but not least, we have to mention two recent experimental works on hunting random zonal flows. The first one was performed at the HT-7 tokamak by Xu [18] and co-workers using specially designed Langmuir probes, detecting floating potential fluctuations. Measuring $\tilde{E}_r$ with a poloidal separation of about 3 cm, they have found a separation in the coherency spectrum identifying the long life ambient turbulence peaking around 50 KHz and a low frequency $<$10 KHz radially localized mode. The second direct ZF identification in a stellarator (CHS) was done very recently in [19] using toroidally separated ($\approx$1.5 m) dual heavy ion beam probes.

Our measurements aim for the identification and detailed characterization of poloidal flow modulations in the CASTOR tokamak. Since poloidal flow fluctuations are connected to the radial electric field through $\tilde{v}_r \simeq \tilde{E}_r/B$ ($\tilde{v}$ denotes velocity fluctuations) there are two possibilities of detecting them:

- measuring fluctuations of the radial electric field;
- direct measurement of the velocity fluctuations by following the movement of turbulence structures in the plasma.

By measuring fluctuations in the radial electric field we have two difficulties. First the available Langmuir probe technique measures a mixture of fluctuations in the potential and the electron temperature: $U_{\mathrm{fl}} \approx \Phi_{\mathrm{pl}} - \alpha T_e$. There is evidence that temperature fluctuations exist in a fusion plasma with similar spatial and temporal behaviour as the potential fluctuations; therefore one can never be sure which component is actually detected. Additionally, the electric field is calculated from the difference between the signals on two floating probes, therefore, the amplitude of the the high-frequency part caused by the turbulence is increased relatively

to the low frequency part. The second problem arises from the required spatial resolution. The radial extent of zonal flows is expected to be approximately equal to the basic turbulence, which is expected to be around the ion Larmor radius. However, the two tips of the measuring probe should be separated by more than the ion Larmor radius so as not to disturb each other. These two requirements contradict each other, therefore, we fear that with properly spaced probes; one would miss a considerable part of the flow structures.

By measuring the flow velocity through the movement of turbulent eddies one assumes that their velocity is dominated by the $E \times B$ flow and not by the velocity of the underlying plasma waves. As will be shown later, we have evidence for this and, additionally, this technique has already been successfully used in several other experiments to detect poloidal flow modulations.

In an optimal case one would need a true 2D measurement to track the movement of eddies in the plasma. The massive holder of these probes would essentially act as a limiter and would probably cause large perturbation to the plasma; therefore, a novel data analysis method was developed which requires only a single radial array of probes. The technique, called the autocorrelation-width technique [20], allows us to extract information on the fluctuations in the flow velocity following the time evolution of the autocorrelation function (ACF) of the basic micro-turbulence.

As detailed below, under certain circumstances, a properly defined quantity, called the autocorrelation-width ($W_{\mathrm{ACF}}(t)$) carries information on the time modulation of the poloidal flow velocity. The characteristic time scale and the spatial structure of the random flow modulation have been deduced from $W_{\mathrm{ACF}}(t)$.

The aim of this paper is to demonstrate the applicability of the autocorrelation width method and to show that zonal flow-like flow modulations do exist in the edge of the CASTOR tokamak plasma.

2. Autocorrelation-width technique

In this section the possibility of detecting B-perpendicular flow modulations by observing temporal variations of the autocorrelation function in a single-point measurement is investigated. In order to calculate the sensitivity of the method we found it essential to analyse the standard deviation of the autocorrelation function due to the finite number of turbulent eddies and/or detector statistical noise. Details of the derivation can be found in [20].

By investigating correlation functions we can get information on the statistical properties of turbulent structures: the correlation time, the correlation length along a spatial coordinate and propagation velocity from the cross-correlation function (CCF). From a very simple model, which deals with poloidally moving structures having Gaussian shape both in space and time, we can calculate the autocorrelation time (it could be measured as the *half-width (FWHM/2)* of the autocorrelation function) in a single-point measurement as a function of the eddy lifetime τ_{life} and the velocity dependent propagation time τ_v:

$$w_t = \frac{\tau_{\mathrm{life}} \cdot \tau_v}{\sqrt{\tau_{\mathrm{life}}^2 + \tau_v^2}}, \tag{1}$$

where $\tau_v = w_\phi / v_\phi$, w_ϕ is the poloidal correlation length and v_ϕ is the poloidal flow velocity. From this formula it is clear that we have two distinct limiting cases:

(a) $\tau_{\mathrm{life}} \gg \tau_v$: for a fixed w_ϕ spatial correlation length the correlation time w_t depends mainly on v_ϕ; $w_t \approx w_\phi / v_\phi$. In this case from the correlation time we can follow the time evolution of the $v_\phi(t)$ flow velocity.

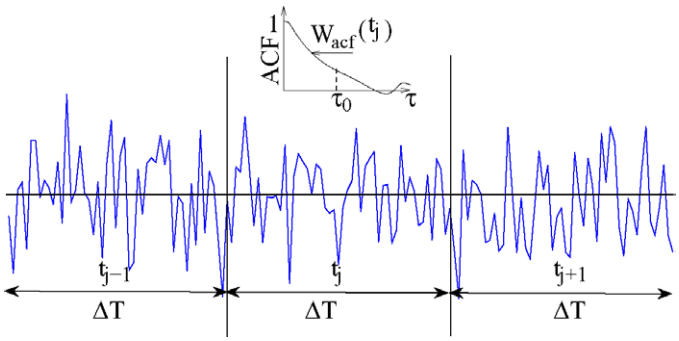

Figure 1. Illustration for the calculation of $W_{\mathrm{ACF}}(t)$. See explanation in the text.

(b) $\tau_{\mathrm{life}} \ll \tau_v$: in this case the correlation time gives information on the eddy lifetime and the flow velocity cannot be deduced.

The heart of the autocorrelation-width technique lies in the validity of the first assumption. In this case the procedure is as follows (see figure 1): first we split the whole time record (T) at shorter ΔT intervals, where the $\Delta T \gg w_t$ relation still holds. Then we calculate autocorrelation functions from these short time intervals and extract information on the width of the autocorrelation function. In this way we obtain the ACF-width (denoted by $W_{\mathrm{ACF}}(t)$) as a function of time with time resolution determined by ΔT. After this procedure we are ready to analyze $W_{\mathrm{ACF}}(t)$ using correlation techniques or spectral methods. It has to be noted that $W_{\mathrm{ACF}}(t)$ can be defined in different ways. In this work, as is described later, W_{ACF} has been taken to be the first moment of the autocorrelation function. To illustrate the feasibility of the method a one plus one dimensional (time and one spatial dimension) simulation was done. Identical Gaussian shaped pulses were moved across a single detection channel with a variable flow velocity. The lifetime (τ_{life}) of these events was much longer than their transit time over the observation volume (τ_v) and the pulses were always generated before reaching the observation. The flow velocity was modulated sinusoidally. In some cases an additional Gaussian noise was added to the signal simulated with a time resolution of 1 μs.

The autocorrelation function was calculated for short time intervals. The effect of the 100 Hz velocity modulation applied in this simulation is clearly observable in figure 2. The power spectrum of the autocorrelation-width signal is shown in figure 2 (bottom) for different relative velocity modulation amplitudes from 0.2 to 0.4. The peak at 100 Hz clearly shows up in all the cases. In one of the plotted cases an additional normally distributed random noise was added with an RMS amplitude identical to the RMS amplitude of the original signal. The resulting power spectrum exhibits a broadband noise and a somewhat reduced sensitivity to the 100 Hz modulation, but the peak is clearly distinguishable.

2.1. Statistics of the autocorrelation function

In order to evaluate the sensitivity of the ACF-width technique described above, an analytical expression was derived [20] for the relative scatter of the autocorrelation function. In our calculation we assume that we have a measured time dependent signal which consists of randomly distributed, limited temporal length events, including overlapping as well. Each event has a time evolution and is described by a set of random variables (with a given but otherwise arbitrary distribution function) such as amplitude, lifetime, time centre. Following the standard definitions the autocorrelation function without normalization (sometimes also

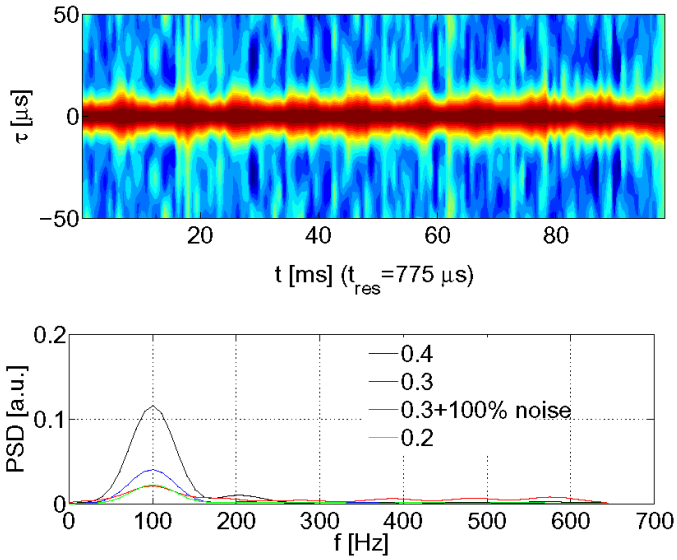

Figure 2. Numerical simulation result illustrating the modulation of the autocorrelation function (top) by the flow and power spectrum of the $W_{\mathrm{ACF}}(t)$ signal for different relative flow modulation amplitudes.

called the autocovariance function) is

$$C_a(\tau) = \overline{[S(t) - \bar{S}] \cdot [S(t+\tau) - \bar{S}]}, \tag{2}$$

where $S(t)$ is the turbulent signal composed of finite lifetime events and the overbar denotes the time average over a given time interval. It can be shown [20] that due to the random appearance of the turbulence events $C_a(\tau)$ at a given time lag τ is a random variable and its variance is independent of τ. After evaluating the statistical averages it is possible to derive an expression for the relative scatter of the autocorrelation function. Using some reasonable assumptions, e.g. a large number of events in one time interval and long integration time relative to the average correlation time ($w_t/\Delta T \ll 1$), we can deduce the following tendency:

$$\frac{\sigma}{\langle C_a(0)\rangle} = D \cdot \sqrt{\frac{w_t}{\Delta T}}, \tag{3}$$

where σ is the standard deviation of the autocorrelation function, $\langle C_a(0)\rangle$ denotes the mean autocorrelation function at zero time lag and D is a constant depending on the details of the distributions of different random variables describing turbulent events. In the case of events with uniform Gaussian shape the value of D can be easily calculated and it was found to be $D = (2\pi)^{1/4}$.

We call this uncertainty 'event statistical noise' as it originates from the finite number of turbulence events in the ΔT interval.

The results of this simple model were compared with real fluctuation measurements (see figure 3) made at the CASTOR tokamak by means of Langmuir probes operating in the ion saturation current regime.

2.2. *Sensitivity to flow velocity modulations*

Having calculated $C_a(\tau)$ for each ΔT long subinterval we need to calculate the autocorrelation time w_t for each of them. According to the limiting case of equation (1) w_t is related to the

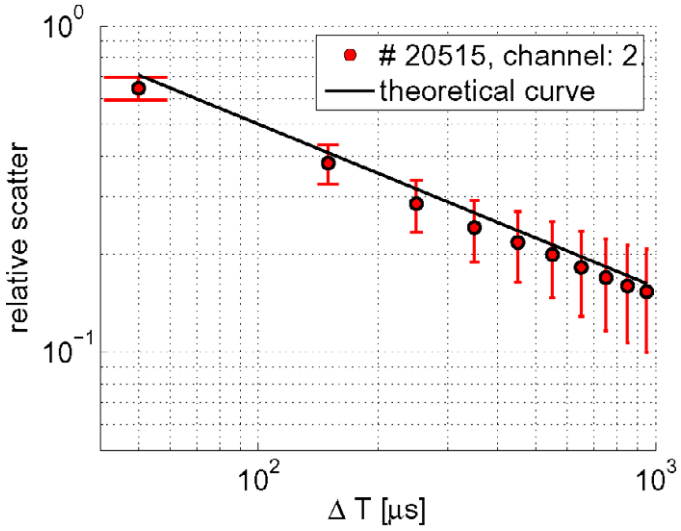

Figure 3. Relative scatter of the autocorrelation function versus integration time ΔT from Gaussian theory and experimental data from fluctuation measurements.

flow velocity through $w_t \approx w_\phi / v_\phi$. As we aim for good time resolution (short ΔT), the autocorrelation function will have a relatively high uncertainity, according to equation (3), typically 20–50%. This high scatter does not allow us to determine w_t as the τ point where $C_a(\tau)$ falls to the half of its maximum. Instead an integral quantity of $C_a(\tau)$ is taken to represent the width of the autocorrelation function. This can be done freely as we are not interested in the actual *value* of w_t but only in its temporal change.

We take the first moment of the autocorrelation function as the measure of the autocorrelation width as

$$W_{\mathrm{ACF}}(t) = \frac{\int_0^{\tau_0} \tau \cdot C_a(\tau)\mathrm{d}\tau}{\int_0^{\tau_0} \cdot C_a(\tau)\mathrm{d}\tau}, \tag{4}$$

where t measures the time evolution over the ΔT subintervals.

Let us suppose that the autocorrelation function has a Gaussian character: $C_a(\tau) \sim \exp\{-(\tau^2/2w_t^2(t))\}$. In this case

$$W_{\mathrm{ACF}}(t) = \frac{\int_0^{\tau_0} \tau \cdot \exp\{-\tau^2/2w_t^2(t)\}\mathrm{d}\tau}{\int_0^{\tau_0} \exp\{-\tau^2/2w_t^2(t)\}\mathrm{d}\tau}. \tag{5}$$

After a simple substitution $\tau' = \tau/\sqrt{2}w_t$ one can get

$$W_{\mathrm{ACF}}(t) = \sqrt{2}w_t(t)\frac{\int_0^{\tau_0/\sqrt{2}w_t} \tau' \cdot \exp\{-\tau'^2\}\mathrm{d}\tau'}{\int_0^{\tau_0/\sqrt{2}w_t} \exp\{-\tau'^2\}\mathrm{d}\tau'} = w_t(t) \cdot A(w_t, \tau_0). \tag{6}$$

In the limit $\tau_0 \to \infty$ $A(w_t, \tau_0)$ becomes independent of w_t and thus

$$\lim_{\tau_0 \to \infty} W_{\mathrm{ACF}} \sim w_t,$$

that is, a certain relative change in w_t will cause the same relative change in $W_{\mathrm{ACF}}(t)$. Of course in a real experimental data processing the integration cannot be extended to infinity but to finite τ_0. In this case the sensitivity of the method decreases according to $A(w_t, \tau_0)$, which

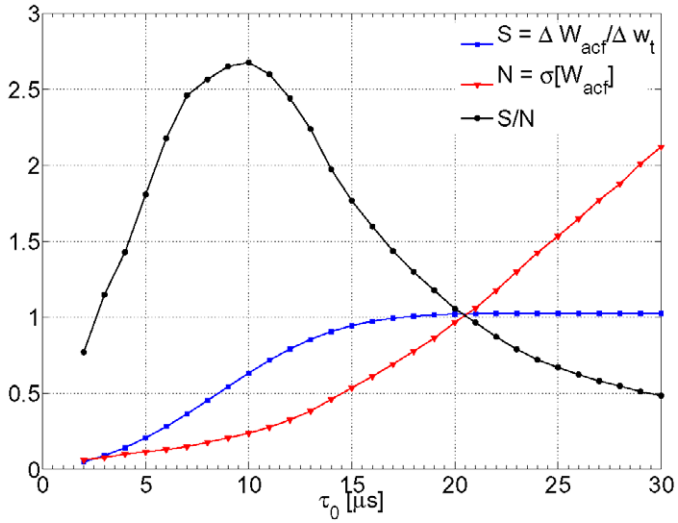

Figure 4. Dependence of the w_t sensitivity (S) and noise (N) of W_{ACF} and the S/N ratio as a function of the integration limit τ_0. The curves are determined from a numerical simulation with $\langle w_t \rangle = 5\,\mu$s and broadband noise amplitude of 50% relative to the fluctuating signal.

can be evaluated numerically as shown in figure 4. by curve 'S'. The selection of τ_0 also affects the noise of W_{ACF}. There are two noise sources: the event statistical noise according to equation (3) and broadband noise from electronics, digitization and other sources. The event statistical noise has w_t autocorrelation time, therefore for $\tau_0 \ll w_t$ it is constant while for large τ_0 it increases approximately with an offset-linear dependence, as shown in figure 4. The contribution of the broadband noise dominates at small τ_0. The simulation result for the overall noise on W_{ACF} as a function of τ_0 for a realistic broadband and event statistical noise level is shown in figure 4. As one can see the S/N ratio has a maximum at approximately $\tau = 10\,\mu$s, which is about twice of w_t. This integration limit is used in the evaluation of the experimental signal.

3. Experimental set-up

Fluctuation measurements were done in the edge plasma of the Ohmic-heated discharges in the CASTOR tokamak [21] ($R = 0.4$ m, $a = 8.5$ cm, $B_t \leqslant 1.5$ T, $I_p \leqslant 25$ kA, $T_{\mathrm{shot}} \leqslant 50$ ms, $\bar{n}_e \leqslant (2-3) \times 10^{19}\mathrm{m}^{-3}$, $T_e(0) \sim 200$ eV), using two *rake probes*, as shown in figure 5. The radial positions of the innermost tips of the vertical and horizontal rake probes with respect to the tokamak center were $r_v = 65$ mm and $r_h = 72$ mm. The two probe arrays were mounted on the same poloidal cross-section. The toroidal angle between the plane of the experiment and the plane of the limiter was 135°, and the radius of the poloidal limiter was 85 mm.

Each rake probe consists of an array of Langmuir-probe tips spaced by 2.5 mm. Odd tips were operated in the *floating potential* regime, while even probe tips were operated in the *ion saturation current* mode. If we make the usual assumption that the temperature fluctuations are negligible, then using the tip-arrangement described above, we are able to measure the radial electric field and the density fluctuations at the same radial positions. From the density (ion saturation current) signal at probe i the autocorrelation-width technique derives the flow

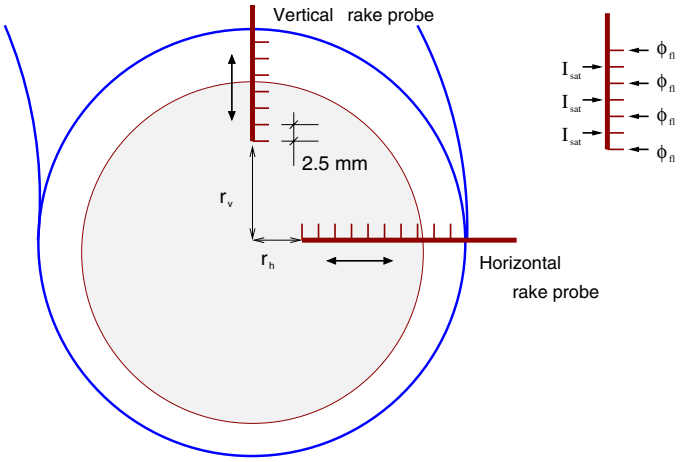

Figure 5. The experimental set-up on the CASTOR tokamak.

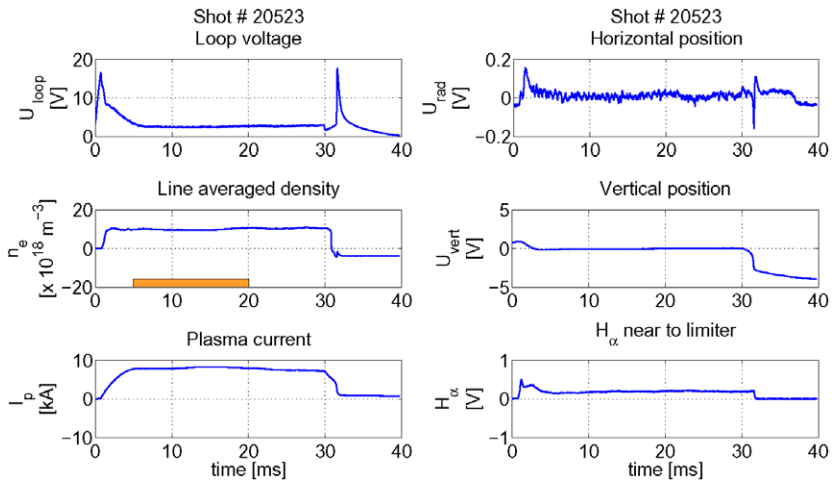

Figure 6. Basic plasma parameters from a typical standard shot in CASTOR. The horizontal bar on the line averaged density plot shows the processing time interval.

velocity modulations at the same location; therefore, we can compare these with the local radial electric field fluctuations at probe i:

$$\tilde{\Phi}_{fl}(i+1) - \tilde{\Phi}_{fl}(i-1) \simeq \tilde{E}_r(i) \sim \tilde{v}(i). \tag{7}$$

In the course of our experimental campaign standard shots ($I_p = 8\,\mathrm{kA}$, $B_T = 1.3\,\mathrm{T}$, $\bar{n}_e \approx 7 \times 10^{18}\,\mathrm{m}^{-3}$) were made. Time evolution of the discharge parameters is shown in figure 6. The plasma was carefully centred in the vessel, which was checked by verifying that the maximum of the floating potential radial profile coincides with the limiter radius. This ensures that we have closed flux surfaces inside the limiter radius [22].

The rake probe signals were sampled at 1 MHz, and for processing we selected a time interval with a length of 15 ms in the stationary phase of the discharges.

Table 1. Shot-to-shot variability of the statistical moments of the ion saturation current fluctuations. The table shows the mean and standard deviation of the statistical moments calculated from the ensemble of 'identical' discharges.

Standard deviation	Kurtosis	Skewness
0.0102 ± 0.0017	3.363 ± 0.176	-0.0059 ± 0.001

4. Signal processing

To analyze the flow modulations the ion saturation current signals were used. They were first filtered numerically with a 3 kHz high-pass filter and subsequently $W_{\mathrm{ACF}}(t)$ was calculated according to equation (4) with $\Delta T = 100\,\mu$s time resolution and $\tau_0 = 10\,\mu$s. The high-pass filter guarantees that no kilohertz scale modulation in the raw signals can enter the analysis, that is, any change in the $W_{\mathrm{ACF}}(t)$ signal should originate from the modulation of the autocorrelation function of the high-frequency component. With these above parameters the ordering of characteristic times is as follows:

$$\Delta t < w_t < \tau_0 \ll \Delta T < T,$$

where Δt is the sampling time (1 μs), w_t is the correlation time of I_{sat} fluctuations (5 μs), τ_0 is the integration time of $C(\tau)$ for the determination of $W_{\mathrm{ACF}}(t)$ (10 μs), ΔT is the length of subintervals (100 μs) and T is the whole analysed time window (15000 μs).

Figure 4 shows a realistic assessment of the signal-to-noise (S/N) ratio and the sensitivity of the $W_{\mathrm{ACF}}(t)$ signal to velocity modulations taking into account both the event statistical noise and broadband noise. From the figure one can see that under the present conditions at about 40% statistical noise is present on the W_{ACF} signal, which is completely uncorrelated between the consecutive time intervals. The response of W_{ACF} to the velocity modulation is reduced to 0.6 due to the finite integration time.

The spatial and temporal behaviour of the flow modulations are analysed in terms of the correlation functions between $W_{\mathrm{ACF}}(t)$ calculated from the rake probe signals measured at different locations.

In order to improve the statistics an ensemble of 21 identical shots were used. Besides comparing global parameters of these discharges, statistical properties of the plasma turbulence were also analyzed to ensure that these experiments were identical in the statistical sense of the turbulence. This means that we have calculated the first four moments of the fluctuating signal for each shot belonging to the ensemble. Table 1 shows the average value and the standard deviation of the moments for the selected shots. (The relative fluctuation amplitude for I_{sat} signals is about 30–40%.)

The first moment is always 0 due to the high-pass filtering. Standard deviation is defined as $\sigma = \sqrt{1/(n-1)\sum_{i=1}^{n}(x_i)^2}$. Skewness is $1/n\sum_{i=1}^{n}(x_i)^3/\sigma^3$ while kurtosis is defined as $1/n\sum_{i=1}^{n}(x_i)^4/\sigma^4$. From the table one can see that the statistical properties are close to Gaussian, and the uncertainty of the first two statistical moments is about 10%. The skewness is always close to zero.

Correlation functions of both the high-frequency ion saturation current fluctuation and the $W_{\mathrm{ACF}}(t)$ signals were calculated for each discharge in the ensemble. Finally the 21 correlation functions were averaged to improve the statistics. After this procedure the autocorrelation at $\tau = 0$ only shows an exceedingly high value. This originates from the fact that the error of the autocorrelation function (see equation (3)) in different, ΔT long subintervals is statistically independent. In order to estimate the correlation value at $\tau = 0$ a linear function was fitted to the correlation values in the $0 < \tau \leqslant 300\,\mu$s range, and the value of this linear fit at $\tau = 0$ was

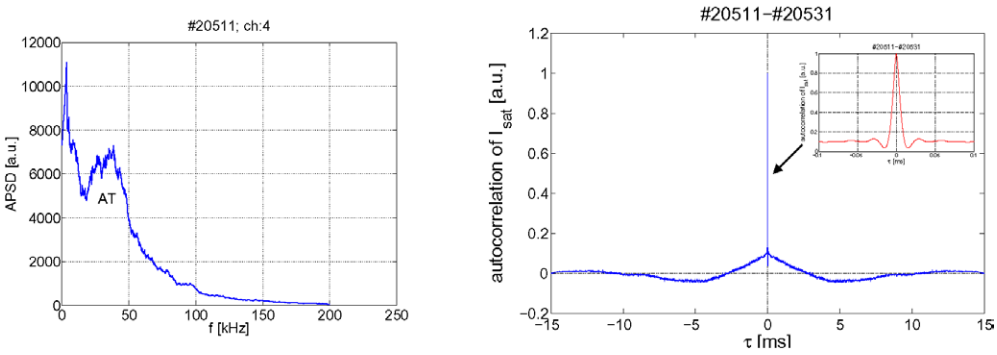

Figure 7. Power density spectrum (left) and autocorrelation (right) of ion saturation current fluctuations on one of the rake probe tips.

taken as $C(\tau = 0)$. For details of this method see [23]. Applicability of this correction assumes that $C(\tau)$ varies slowly in this τ-range, which is clear from figure 11(*c*). For normalization of the correlation functions this extrapolated $\tau = 0$ autocorrelation value was used:

$$C_{12}^{N}(\tau) = \frac{C_{12}(\tau)}{\sqrt{C_{a,1}(0)C_{a,2}(0)}}. \tag{8}$$

Here $C_{12}^{N}(\tau)$ and $C_{12}(\tau)$ are the correlation functions of two signals with and without normalization, respectively. $C_{a,i}(0)$ is the noise peak corrected value of the autocorrelation function at $\tau = 0$ of ith signal.

5. Results

5.1. Time-scale separation

The ion saturation current rake probe signals were analysed from several points of view. First power spectra and correlation functions were used to analyze the temporal and spatial characteristics of the turbulence with a typically 5 μs correlation time.

Figure 7 shows a power spectrum and autocorrelation of a selected rake probe signal before applying the 3 kHz high-pass filter. Two distinct time scales are seen: on the one hand the basic micro-turbulence (designated by 'ambient turbulence', (AT)), characterized by 30–100 kHz frequencies and on the other hand a pronounced peak is present at lower frequencies. The origin of this low frequency part is unknown. ZFs are expected to have no associated density modulation, but as they can regulate turbulence and transport they might modulate the density through this latter link. Alternatively, external sources might also modulate the density through, e.g. changes in the gas flow rate. These possibilities are not analysed in the current paper and therefore the low frequency component was removed by numerical filtering.

5.2. Characterization of the basic micro-turbulence

In the previous section it was pointed out that the autocorrelation-width technique can be used only if the autocorrelation time of the basic turbulent structures is dominated by the poloidal flow velocity. In order to check this statement first the transit time $\tau_v = w_\phi / v_\phi$ was calculated. The typical poloidal size of the ion saturation turbulence structures was found to be about 1.5 cm in the whole edge plasma [21]. In some recent measurements the poloidal flow velocity at the edge region was deduced from the shift of the cross-correlation maximum between two

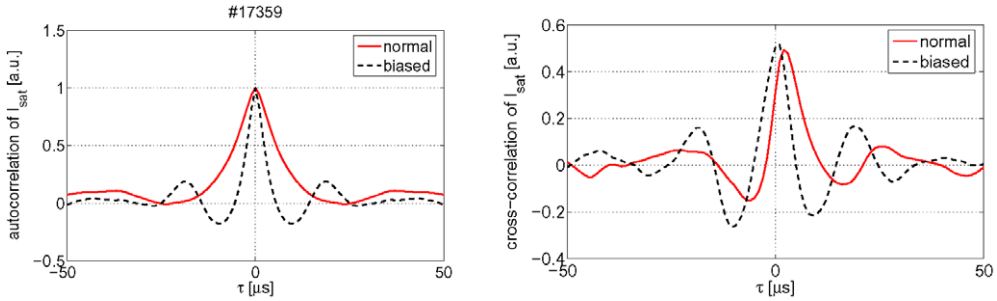

Figure 8. Autocorrelation and crosscorrelation function for the poloidally displaced Langmuir probes. The solid line shows correlation in standard shot, the dashed line in biased experiment.

poloidally separated Langmuir probes. It was found that the poloidal flow velocity always exceeds $3\,\mathrm{km\,s^{-1}}$, from which the transit time of the structures lies close to the measured autocorrelation time.

To further check that the transit time determines the width of the ACF (case (a) in the discussion following equation (1)) the radial electric field was increased by applying edge biasing, which also results in an increase in poloidal rotation velocity. Autocorrelation functions (figure 8 (left)) and cross-correlation functions (figure 8 (right)) of the ion saturation current fluctuations between two poloidally separated probes are shown for two cases: a standard discharge and a time window when the edge plasma potential was biased. The plots clearly show roughly a doubling of the shift of the maximum of the CCF: $\Delta\tau^{\mathrm{standard}}/\Delta\tau^{\mathrm{bias}} = 2.5$ (the plot on the right-hand side—the red line) in the non-biased case, indicating half velocity. At the same time the autocorrelation time is about double in the non-biased case compared with the biased one: $w_t^{\mathrm{standard}}/w_t^{\mathrm{bias}} = 2.4$ (the plot on the left-hand side—the dashed red line). The response of the autocorrelation time to the velocity increase in the biased plasma supports the above calculations that the autocorrelation time is determined by the transit time of turbulent structures; therefore the autocorrelation-width method is applicable.

The temporal behaviour of the high frequency fluctuations of the plasma which are associated with the small scale plasma turbulence is shown in figure 9. From the fluctuation measurements of both the floating potential ($\tilde{\Phi}_f$) and the ion saturation current ($\tilde{I}_{\mathrm{sat}}$) one can draw the following conclusion for features of ambient turbulence: the characteristic time scale is a couple of microseconds, while the radial correlation length is found to be $\approx$1 cm. These features are in agreement with the results obtained in other devices. Figure 9 shows that there is a small correlation between fluctuations measured in the two different rake probes. This is generally true between all the tips, which means that structures of the basic microturbulence do not have a long enough lifetime to cover the 90° poloidal distance between the two rake probes. Although toroidal correlation measurements were not performed in the experiments presented in this paper, we have information from some more recent measurements. Typically the value of the correlation is 0.8, which can be found over about 1 m (half-toroidal turn) distance between the two probes if they are precisely located in the same flux tube.

5.3. Correlation analysis of $W_{\mathrm{ACF}}(t)$

The $W_{\mathrm{ACF}}(t)$ signal for a selected shot is shown in figure 10. The broadband noise dominates the fluctuations as expected, but lower frequency changes are also discernible. After the calculation of the autocorrelation function of $W_{\mathrm{ACF}}(C_a^W)$ it is corrected for this broadband

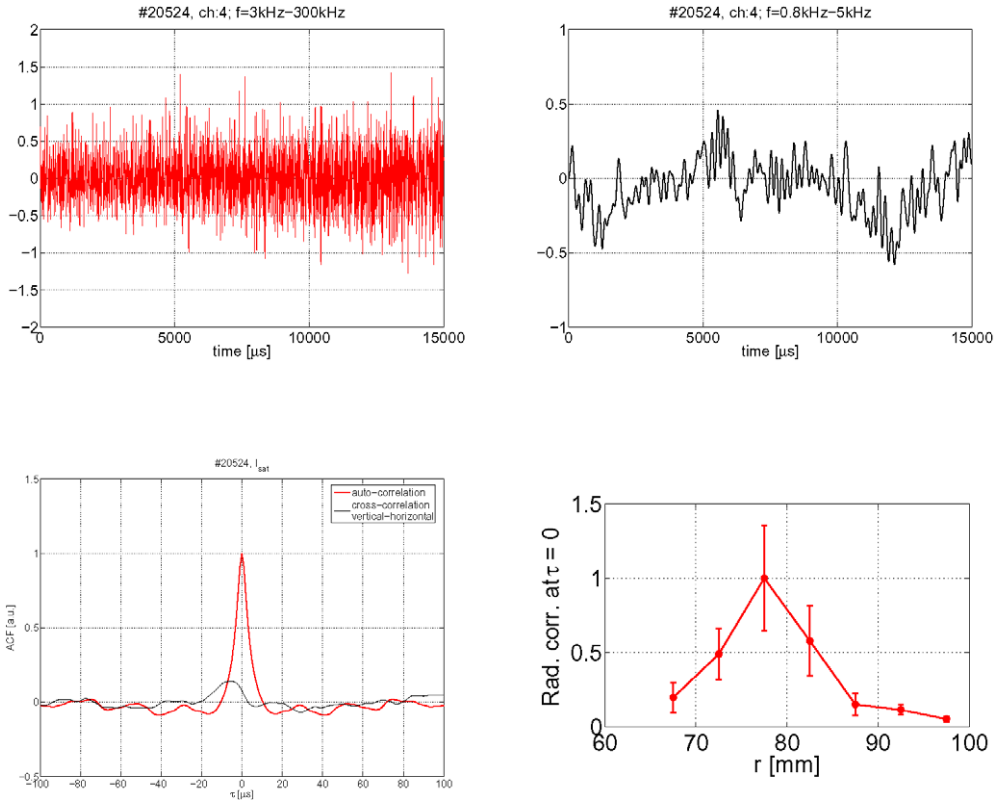

Figure 9. Raw signal for fast scale (top left) and slow scale (top right) $I_{\rm sat}$ fluctuations. The autocorrelation function at $r/a = 0.88$ and the cross-correlation function between vertical and horizontal rake probes (bottom left). The radial distributon of correlation at zero time lag for the fast scale $I_{\rm sat}$ fluctuations (bottom right).

noise by extrapolation as described at the end of the section on signal processing. The relative RMS amplitude of the low-frequency modulations is calculated as

$$R = \frac{\sqrt{C_a^W(0)}}{\overline{W_{\rm ACF}(t)}}. \tag{9}$$

In the above expression $\overline{W_{\rm ACF}}$ is the time average of $W_{\rm ACF}$ and $C_a^W(0)$ means the noise peak corrected autocorrelation function of $W_{\rm ACF}$. The value of R appears to be about 0.1–0.15. This relative amplitude is plotted for all discharges in the bottom plot of figure 10. The RMS relative modulation amplitude is well reproduced, the average being 13%. According to simulations the relative sensitivity of $W_{\rm ACF}$ to velocity modulations is 0.6 (see figure 4), therefore the velocity modulation amplitude is expected to be about 20%.

The results of the correlation calculation for $W_{\rm ACF}(t)$ can be seen in figure 11. The left-hand side of the figure shows the characteristic time scale of flow modulations (bottom) to be ∼1 ms, and the radial structure of the random flows (top) which clearly indicates radial localization (1 cm width) in the edge plasma. Plots on the right-hand side show the cross-correlation between a given reference channel located at the horizontal probe and all other channels at the vertical probe. The high cross-correlation indicates that the flow structures remain significantly correlated in the poloidal direction even when measurement channels are separated by 12 cm (90°).

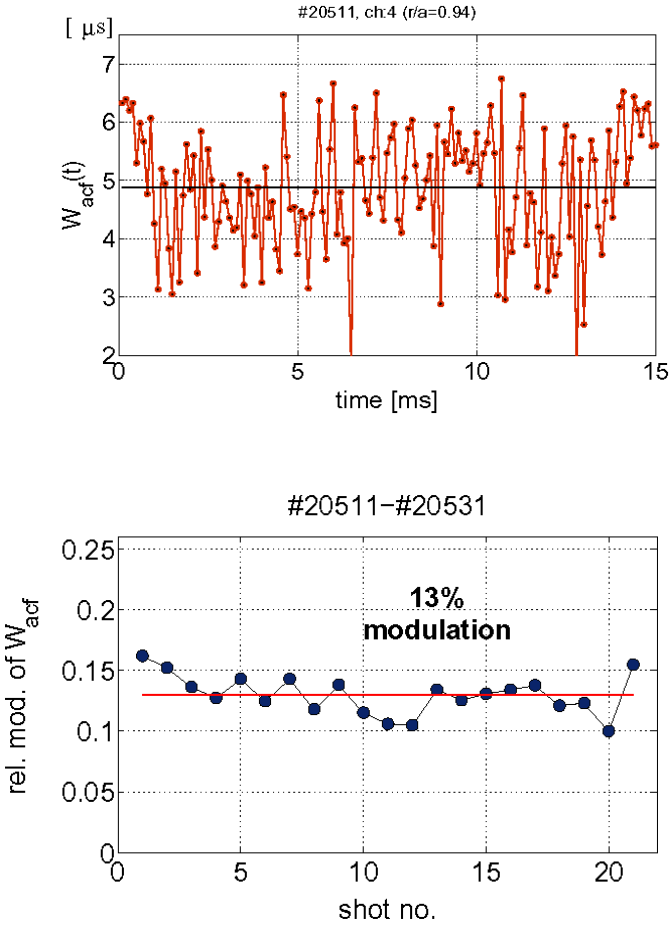

Figure 10. Time evolution of W_{ACF} (top) in a selected discharge. Its relative modulation after correction for the statistical noise is shown for all 21 identical discharges on the bottom plot.

One can estimate the statistical error of the correlation functions using equation (3). Although the shape of the correlation peak is not exactly Gaussian a rough estimation can be made as the signal consists of about 1 ms wide events. Using $w_t \approx 1$ ms for the correlation time of the flow modulation events and $T_{\mathrm{meas}} \approx 300$ ms for the total measurement time in the 21 identical shots, we can get $\sigma/C \approx 0.1$ as the relative error originating from the finite number of detected events. This value is in reasonable agreement with the modulation of the correlation functions at long time lags.

As the energy confinement time in the CASTOR tokamak is typically 1 ms, it appears essential to check whether the observed flow velocity modulations originate from global plasma changes or from relevant local features. To this end correlations between ACF-width signals and relevant global parameters (loop voltage(U_{loop}), horizontal and vertical plasma position) are plotted in figure 12. There are no systematic correlated changes in the global plasma parameters and modulations in the flow velocity.

The present experimental set-up allowed measurements of the radial electric field fluctuations and density fluctuations at the same radial position. Hence it is possible to directly check the correlation between the W_{ACF} and $\tilde{E}_r$. Fluctuations in the latter are expected to be

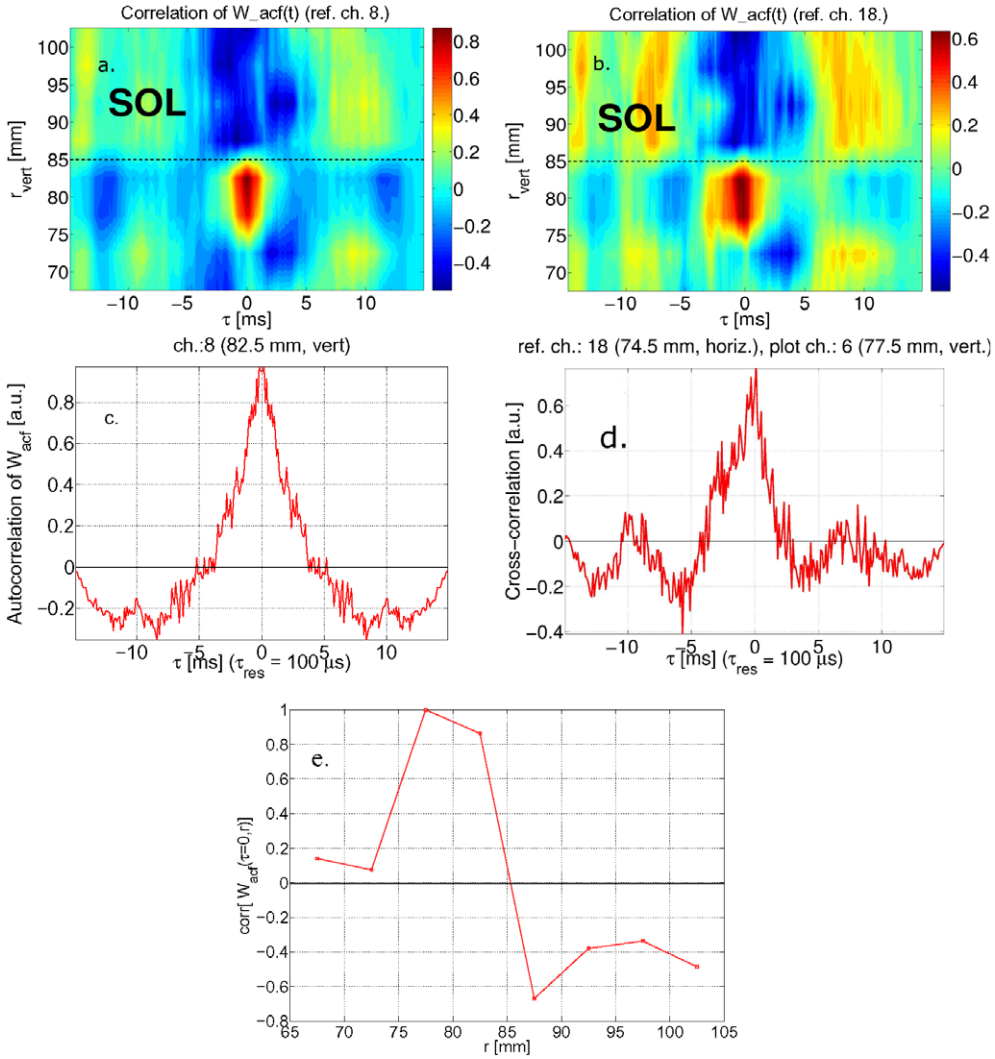

Figure 11. Space-time correlation structure of flow modulations averaged over 21 identical shots. (*a*) Radial–temporal correlation function of noise peak corrected W_{ACF} along the vertical rake probe, where r_{vert} is the distance from the center of the device and τ is the time lag; (*b*) cross-correlation function of W_{ACF} along the vertical rake probe with the reference channel at the horizontal rake probe; (*c*) autocorrelation function of W_{ACF} at one location in plot (*a*); (*d*) cross-correlation between two channels located at different rakes at the same radial position and (*e*) the radial distribution of correlation at zero time lag. (The reference position was 77.5 mm.)

directly connected to the fluctuations in the poloidal flow velocity. The result is plotted in figure 13. A peak is indeed seen around 0 time lag, however, with a relatively low normalized amplitude.

6. Discussion

The results described above indicate the existence of radially localized and poloidally extended random flow structures with about 1 ms lifetime in the CASTOR tokamak. The poloidal

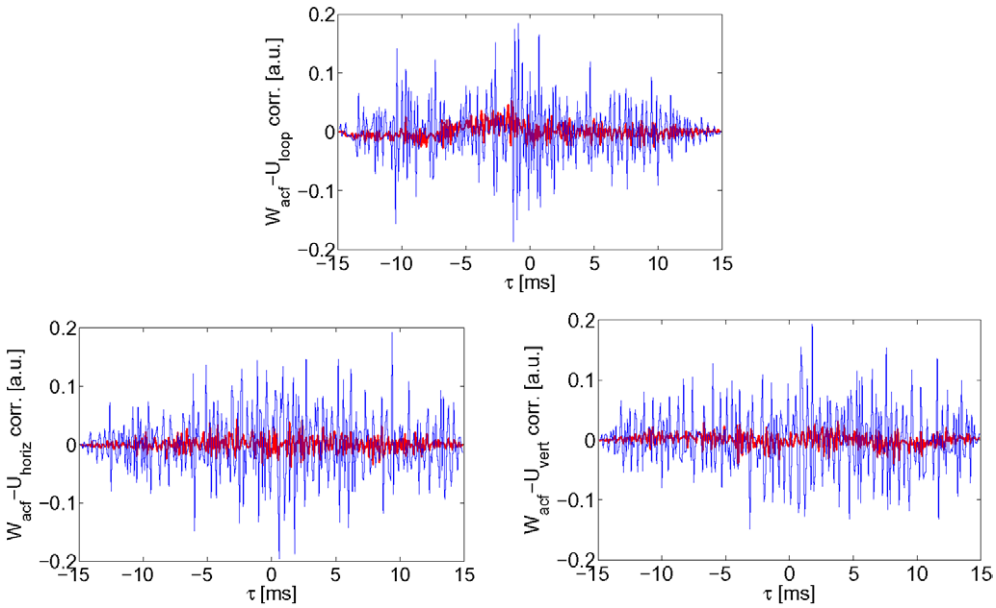

Figure 12. Correlations between the W_{ACF} signal and some global parameters: loop voltage, horizontal and vertical plasma position. The strongly fluctuating correlations are calculated from one discharge; the thick lines indicate averages over the ensamble of 21 discharges.

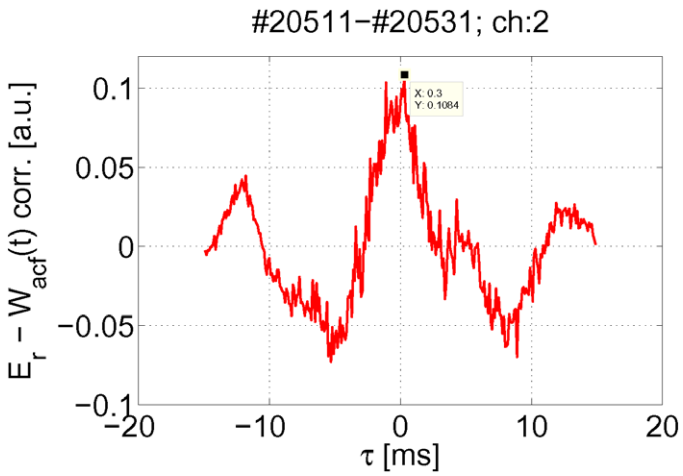

Figure 13. Cross-correlation function between radial electric field fluctuations $\tilde{E}_r$ and the W_{ACF} signal.

correlation is around 0.7 over the 90° poloidal angle which is definitely not carried by the basic turbulence structures themselves, as no direct correlation is observed in the turbulence between the two rake probes. There is no direct information on the toroidal correlation of the flow structures, but around 0.8 correlation can be observed in CASTOR in the basic microturbulence along a flux tube extending over the half major circumference, the flow modulations (derived from the analysis of these long correlated structures) should also have a high toroidal symmetry.

The lifetime of the flow structures is close to the global confinement time in the tokamak; therefore, one could argue that they might be a result of some global plasma changes. This is excluded by the fact that no correlation is observed between the flow modulation and some global plasma parameters.

The experimental arrangement enables the determination of the correlation between the radial electric field (from the difference in the floating potential at two radially offset Langmuir probes) and the flow modulations at the same location in the plasma. Correlation between these signals indeed shows a peak around 0 time lag with about 1 ms width, but the amplitude of the correlation is rather low, only around 0.1. This might be caused by two factors:

- the electric field is measured as the difference between signals of two floating probes offset radially by 5 mm. One might argue that part of the flow structures with similar widths might be missed by the electric field measurement. A numerical simulation of Gaussian potential structures with a fixed radial width and random location excluded this possibility. In the case of a radial width agreeing with the experimentally observed flow structure width there should be high correlation with the electric field. To get low correlation with the electric field one would need such narrow radial structures which contradict the experiment;
- the floating potential measurement contains a contribution from the plasma temperature as well. If there are millisecond timescale modulations in the temperature which are uncorrelated with the flow modulations, they will reduce the amplitude of the observed correlation between the electric field and the flow. Unfortunately no temperature measurement was available on CASTOR with the required spatial and temporal resolution, but such low-frequency oscillations are indeed observed in the ion saturation current (see figure 7), and they showed no correlation with the flow modulations. If these low-frequency density fluctuations originate from external sources, e.g. fluctuations in the gas flow rate to the plasma, they should also cause some low-frequency temperature fluctuations which are also not correlated with the flow modulations. Such additional temperature modulations will appear in the electric field measurement through the floating potential and it will reduce the correlation with the flows. We think this mechanism can be a real cause, but unfortunately no direct observations are available to prove it.

7. Conclusion

Detailed fluctuation measurements were made in Ohmic-heated discharges of the CASTOR tokamak. Ion saturation current and potential fluctuations were detected using two radial arrays of Langmuir probes (rake probes), located in the same toroidal cross-section at 90° poloidal angle relative to each other. The characteristics of the basic microturbulence were found to be similar to the observations on other devices: some microsecond correlation time and about 1 cm radial correlation length. Modulation in the poloidal flow velocity of these microturbulence structures was determined using a new numerical technique which follows the time evolution of the autocorrelation function of single-point measurements. The existence of ∼20% RMS amplitude modulations in the poloidal flow were revealed, which are radially well localized (∼1 cm) and poloidally highly correlated, although the basic microturbulence has typically only 1.5 cm poloidal correlation length. These flow structures have a characteristic lifetime of ∼1 ms. Some correlation between the flow measurements using the new technique and modulation in the radial electric field was also determined. Although the lifetime of the flow structures is close to the energy confinement time of the CASTOR tokamak plasma, no

correlation could be observed between the flows and global plasma parameters; therefore the former are not a consequence of the global plasma condition changes.

All the above mentioned features of the detected flow structures strongly suggest the appearance of zonal flows described by theory as $m = 0, n = 0$ radially localized random potential structures. Our results are also consistent with the recent experimental work reported in [19].

References

[1] Yoshizawa A, Itoh S, Itoh K and Yokoi N 2001 *Plasma Phys. Control. Fusion* **43** R1–144
[2] Diamond P H, Itoh S, Itoh K and Hahm T S 2005 *Plasma Phys. Control. Fusion* **47** R35–161
[3] Holland C *et al* 2003 *Nucl. Fusion* **43** 761
[4] Dimits A M *et al* 2000 *Phys. Plasmas* **7** 969
[5] Lin Z and Hahm T S *et al* 1998 *Science* **281** 1835
[6] Rogers B N, Dorland W and Kotschenreuther M 2000 *Phys. Rev. Lett.* **85** 5336
[7] Hammett G W, Beer M A, Dorland W, Cowley S C and Smith S A 1993 *Plasma Phys. Control. Fusion* **35** 973
[8] Hidalgo C, Silva C, Pedrosa M A, Sanchez E, Fernandes H and Varandas C A F 1999 *Phys. Rev. Lett.* **83** 2203
[9] Xu Y H, Yu C X, Luo J R, Mao J S, Liu B H, Li J G, Wan B N and Wan Y X 2000 *Phys. Rev. Lett.* **84** 3867
[10] Vianello N, Spada E, Antoni V, Sopolare M, Serianni G, Regnoli G, Cavazzana R, Bergsaker H and Drake J R 2005 *Phys. Rev. Lett.* **94** 135001
[11] Diamond P H *et al* 2000 *Phys. Rev. Lett.* **84** 4842
[12] Holland C, Tynan G R, Diamond P H, Moyer R A and Burin M J 2002 *Plasma Phys. Control. Fusion* **44** A453–7
[13] Moyer R A, Tynan G R, Holland C and Burin M J 2001 *Phys. Rev. Lett.* **87** 135001
[14] Coda S, Porkolab M and Burell K H 2001 *Phys. Rev. Lett.* **86** 4835
[15] Jakubowski M, Fonck R J and McKee G R 2002 *Phys. Rev. Lett.* **89** 265003
[16] Hallatschek K and Biskamp D 2001 *Phys. Rev. Lett.* **86** 1223
[17] Conway G D, Scott B, Schirmer J, Reich M, Kendl A and ASDEX Upgrade Team 2005 *Plasma Phys. Control. Fusion* **47** 1165
[18] Xu G S, Wan B N, Song M and Li J 2003 *Phys. Rev. Lett.* **91** 125001
[19] Fujisawa A *et al* 2005 *Phys. Rev. Lett.* **93** 165002
[20] Bencze A and Zoletnik S 2005 *Phys. Plasmas* **12** 052323
[21] Hron M *et al* 1999 *Czech. J. Phys.* **49** 181
[22] Devynck P *et al* 2005 *Plasma Phys. Control. Fusion* **47** 269
[23] Zoletnik S, Fiedler S, Kocsis G, McCormick G K, Schweinzer J and Winter H P 1998 *Plasma Phys. Control. Fusion* **40** 1399